Geophysical Journal International

Geophys. J. Int. (2012) **191,** 579–590 doi: 10.1111/j.1365-246X.2012.05635.x

1-D and 2-D resonances in an Alpine valley identified from ambient noise measurements and 3-D modelling

Olivier Le Roux,[1] Cécile Cornou,[2] Denis Jongmans,[2] and Stéphane Schwartz[2]

[1] *Géoressources et Environnement (*EA 4592*), Université de Bordeaux,* 1 *allée Daguin,* 33607 *Pessac cedex, France. E-mail: Olivier.Le_Roux@ensegid.fr*
[2] *ISTerre, CNRS, Université Joseph Fourier, IRD, Grenoble* 1, BP 53, 38041, *Grenoble cedex* 09, *France*

Accepted 2012 July 30. Received 2012 July 23; in original form 2011 October 4

SUMMARY

H/V spectral ratios are regularly used for estimating the bedrock depth in 1-D like basins exhibiting smooth lateral variations. In the case of 2-D or 3-D pronounced geometries, observational and numerical studies have shown that H/V curves exhibit peculiar shapes and that the H/V frequency generally overestimates 1-D theoretical resonance frequency. To investigate the capabilities of the H/V method in complex structures, a detailed comparison between measured and 3-D-simulated ambient vibrations was performed in the small-size lower Romanche valley (French Alps), which shows significant variations in geometry, downstream and upstream the Séchilienne basin. Analysing the H/V curve characteristics, two different wave propagation modes were identified along the valley. Relying on previous geophysical investigation, a power-law relationship was derived between the bedrock depth and the H/V peak frequency, which was used for building a 3-D model of the valley geometry. Simulated and experimental H/V curves were found to exhibit quite similar features in terms of curve shape and peak frequency values, validating the 3-D structure. This good agreement also evidenced two different propagation modes in the valley: 2-D resonance in the Séchilienne basin and 1-D resonance in the external parts. This study underlines the interest of H/V curves for investigating complex basin structures.

Key words: Fourier analysis; Numerical solutions; Geomorphology; Site effects; Wave propagation; Sedimentary basin processes.

1 INTRODUCTION

Sedimentary basins are widespread and most often consist of low-velocity sediments overlying more rigid bedrock. Such structures are prone to resonance phenomena, which are mainly controlled by the contrast in shear wave velocities between sediments and seismic bedrock and the thickness of the sediment layer. For a horizontally 1-D layered structure, both amplification and fundamental resonance frequency ($f_0^{1\text{-D}}$) can thus be easily computed if the shear wave velocity is known in sediments and underlying bedrock. However, both earthquake ground motion records and numerical modelling studies have demonstrated the significant role of 2-D or 3-D geometries on site effects, generating surface waves and yielding large signal duration and amplification far beyond the level predicted using 1-D structures (e.g. Bard & Bouchon 1985; Moczo & Bard 1993; Sánchez-Sesma & Luzón 1995; Field 1996; Kawase 1996; Graves *et al.* 1998; Chávez-Garcia *et al.* 2000; Rovelli *et al.* 2001; Chávez-Garcia *et al.* 2003; Cornou & Bard 2003; Bindi *et al.* 2009).

In the last 20 years, ambient noise has been increasingly used for site effects studies and characterization of geological structures. In particular, the H/V spectral ratio technique (Nogoshi & Igarashi 1972; Nakamura 1989) has become a popular tool in earthquake engineering. The success came from the correlation observed between the H/V peak frequency (f_{HV}) and the fundamental resonance frequency of the site (e.g. Bard 1998; Haghshenas *et al.* 2008). Although the fundamentals of the H/V technique are still debated (Lermo & Chávez-García 1994; Malischewsky & Scherbaum 2004; Bonnefoy-Claudet *et al.* 2006a; Albarello & Lunedei 2009; Lunedei & Albarello 2010; Tuan *et al.* 2011; Sánchez-Sesma *et al.* 2011), this technique has been successfully used for mapping bedrock depth in sediment-filled basins (among others, Ibs-von Seht & Wohlenberg 1999; Delgado *et al.* 2000; Parolai *et al.* 2002; Hinzen *et al.* 2004; Benjumea *et al.* 2011; Bièvre *et al.* 2011; Özalaybey *et al.* 2011), using the relation between fundamental resonance frequency (f_0), average shear wave velocity (β) and thickness of sediments (H) ($f_0 = \beta/4H$). Since shear wave velocity profiles are not always available, authors most often calibrate locally a power-law relationship that relates fundamental resonance frequency (f_{HV}) and sediments thickness (H).

While in 1-D structures H/V ratios usually show a well-defined peak, especially for large impedance contrasts, H/V curves exhibit more complex shape in 2-D and 3-D structures, which makes debatable the use of H/V peak frequencies for imaging purposes in such structures. By comparing Rayleigh ellipticity curves based on 1-D stratified models with H/V ratios observed in the Osaka basin,

Uebayashi *et al.* (2003) found different shape and peak frequencies in areas above strong irregular basement depths and/or close to the basin edge. Such complexity with a broad H/V peak of low amplitude was also explicitly reported in Santiago (Chile) (Bonnefoy-Claudet *et al.* 2009), in Colfiorito (Italy) (Di Giulio *et al.* 2006), in the Izmit basin (Turkey) (Özalaybey *et al.* 2011) and in Spain (Benjumea *et al.* 2011). Numerical modelling of ambient noise in various 2-D and 3-D structures (Guillier *et al.* 2006) have outlined that H/V curves exhibit well-defined peaks in the flat parts of 2-D/3-D structures but broad peaks or plateau-like shapes of low amplitude close to the valley edges. For such plateau-like H/V curves, they suggest to peak the frequency at the plateau cut-off. Guillier *et al.* (2006) confirmed that the H/V peak frequency corresponds to the 1-D resonance frequency in the flat part of the valley but systematically deviates from the 1-D resonance frequency near the valley edges, depending on the valley shape ratio defined as the ratio between the maximal sediment thickness and the width of the valley at mid-depth (Bard & Bouchon 1985). They also concluded that, although H/V curves having broad peaks or plateau-like shapes testify to the complexity in the underground structure, they should not be used for deriving any quantitative information of underground structure by using the simple $f_0 = \beta/4H$ relation. In 2-D deep valleys having a large shape ratio (thickness/half-width >0.3) like in the deep Rhône valley (Swiss Alps) (Roten *et al.* 2006) or in the Grenoble Basin (France) (Guéguen *et al.* 2007), significant differences were observed between the theoretical 1-D resonance frequency and H/V peak frequencies, the latter systematically overestimating the theoretical resonance frequency in the valley centre, as a consequence of 2-D resonance. These authors showed that 2-D resonance modes created prominent peaks in H/V ratios, which cannot be interpreted in terms of 1-D resonance.

To our knowledge, although relations between shape of H/V curve and wave propagation at play have been frequently observed or modelled, a detailed comparison between ambient noise measurements recorded in a complex basin and noise numerical simulations has not yet been performed. The aim of this paper is thus to better investigate correlation between H/V curve shape and wave propagation by means of experimental and numerical approaches and to derive a strategy for the application of the H/V technique for deep basin investigation. The chosen site is a 5 km long section in the lower Romanche glacial valley (French Alps), which was geophysically and morphologically investigated by Le Roux *et al.* (2010) and Le Roux (2011). The valley exhibits significant variations in width and depth, resulting from lithological changes and fault crossing. Ambient noise measurements were performed along different profiles along and perpendicular to the valley axis. A 3-D seismic model of the valley was defined by using a power-law relationship correlating H/V peak frequencies derived from ambient noise measurements and bedrock depth estimated by other geophysical methods. The analysis of the experimental and numerical H/V curve characteristics allow distinguishing 1-D and 2-D wave propagation modes along the valley.

2 GEOLOGICAL AND GEOPHYSICAL SETTINGS

The study area is located in the south-western part of the Belledonne Massif, a Palaeozoic External Crystalline Massif of the French western Alps (Fig. 1). It is crosscut by the NS-trending near-vertical Belledonne Middle Fault (*BMF*) (Fig. 1b) which separates the western external micaschist domain from the eastern internal domain made of amphibolites andgneisses (Fig. 1b; Barféty *et al.* 1972; Guillot *et al.* 2010). These metamorphic rocks are locally unconformably covered with Mesozoic carbonate sediments and Quaternary deposits (scree and fluvial deposits, alluvial cone, moraines). In this area, the Belledonne massif is carved by the

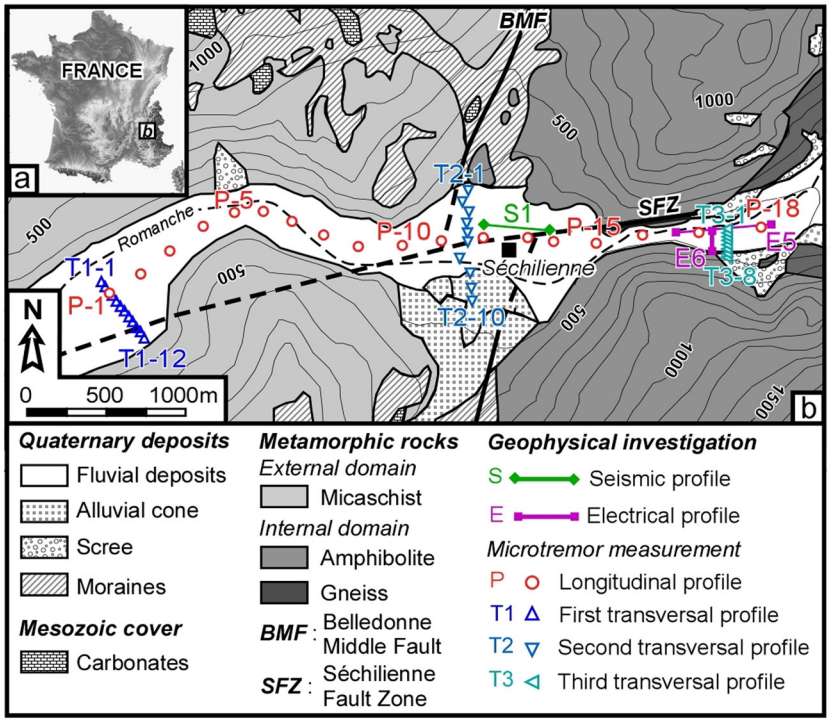

Figure 1. (a) Location of the study area (southern part of the Belledonne Massif, France). (b) Geological and structural map with the location of the geophysical investigations (modified from Barféty *et al.* 1972).

east–west trending lower Romanche valley filled by glacio-alluvial sediments (Fig. 1b). This incision results from the alternate activity of the Romanche River and the Romanche glacier during the Quaternary glaciations (Montjuvent & Winistorfer 1980; Le Roux *et al.* 2010).

At the intersection with the *BMF*, the Romanche valley widens in the kilometre size lozenge-shaped basin of Sechilienne (Fig. 1b). Recent geological and geophysical investigation (Le Roux *et al.* 2010; Le Roux 2011) has revealed the existence of a N80 sinistral strike-slip fault zone (*SFZ*), offsetting the *BMF* by 375 m, and of a significant valley floor overdeepening (from 100 to 370 m depth) across the Séchilienne basin. No sign of recent activity along the *SFZ* was evidenced by these studies. That suggests that the Séchilienne basin geometry results mainly from the Quaternary glacial erosion across a major lithological contrast, between amphibolites to the east and more erodable micaschists to the west. The rock erodability in the zone was probably magnified by the intersection of the two faults (*BMF* and *SFZ*; Le Roux *et al.* 2010). A shallower overdeepening (from 100 to 170 m) was also observed in the eastern prolongation of the *SFZ*, upstream the Séchilienne basin. These strong valley floor depth variations, along with local valley broadening, make the lower Romanche valley a good candidate site for studying resonance effects from ambient vibrations in a non-1-D structure.

3 AMBIENT NOISE MEASUREMENTS

One longitudinal profile of 18 single-station ambient noise measurements was acquired along the Romanche valley, from downstream to upstream the Séchilienne basin (profile P, Fig. 1b). Three transversal profiles labelled T1, T2 and T3, making use of 8–12 stations, were also deployed downstream, into and upstream the Séchilienne basin, respectively (Fig. 1b). Microtremor acquisition was performed during 30 min by using Cityshark@ acquisition unit connected to a 5-s Lennartz sensor. H/V spectral ratios were computed by using the Geopsy software (http://www.geopsy.org; Wathelet *et al.* 2008). Noise recordings were cut in most stationary time windows ranging from 30 to 60 s duration length by using a STA/LTA anti-triggering algorithm. Fourier amplitude spectra were then smoothed using the processing proposed by Konno & Ohmachi (1998) with $b = 40$ and the two horizontal components were combined by computing the quadratic mean. H/V ratios at each station are then computed by averaging the H/V ratios obtained on individual windows. The four H/V profiles derived from ambient noise measurements are displayed in Fig. 2. H/V peak frequencies along transverse profiles exhibit variations that are obviously correlated to the bedrock depth, lower H/V peak frequencies being found at the valley centre (Figs 2b–d). However, H/V curves along the longitudinal profile

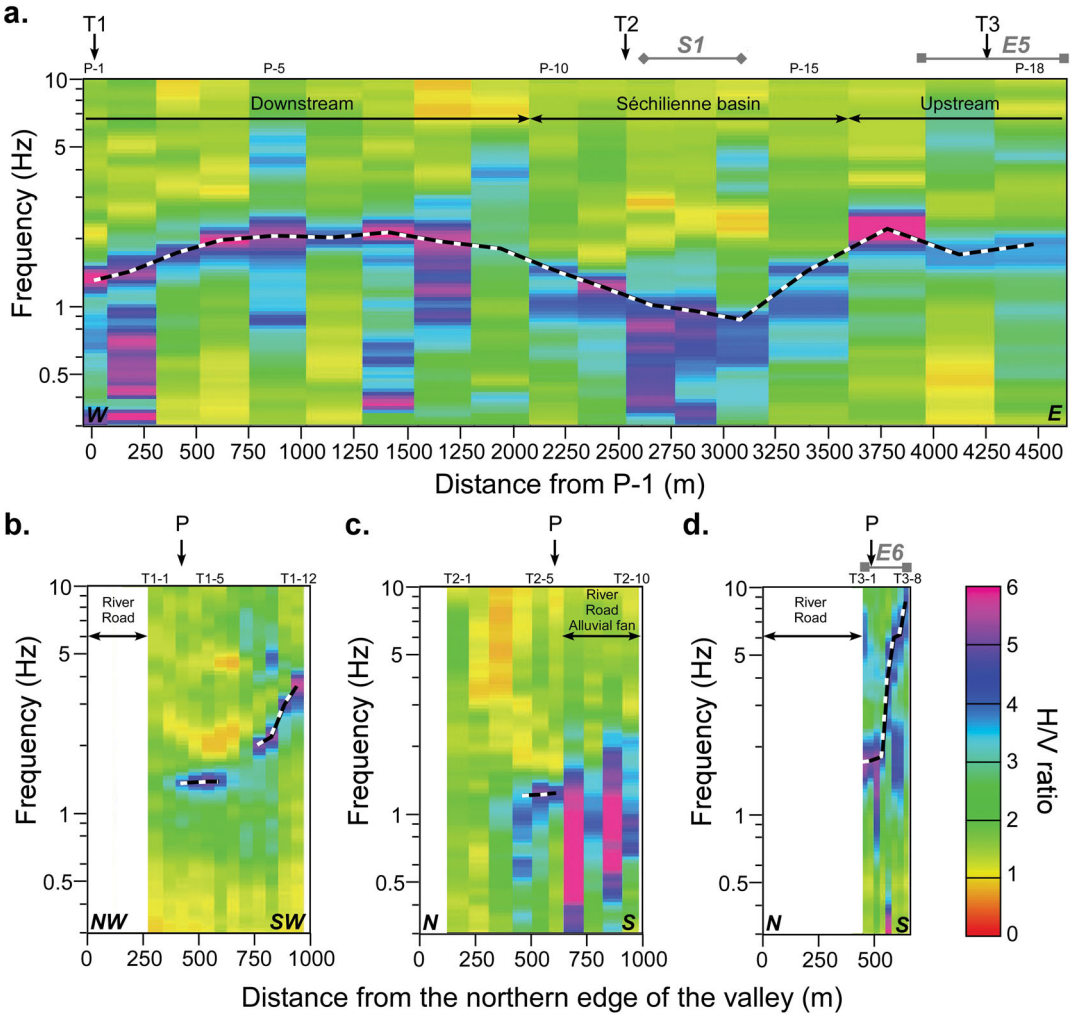

Figure 2. H/V spectral ratios computed from ambient noise measurements. (a) Longitudinal H/V profile along the Romanche valley (profile P). (b) First transversal H/V profile (profile T1). (c) Second transversal H/V profile (profile T2). (d) Third transversal H/V profile (profile T3). Dotted line: H/V peak frequencies (f_{HV}^{M}). S1: seismic reflexion profile carried out by Le Roux *et al.* (2010). E5 and E6: electrical profiles carried out by Le Roux (2011).

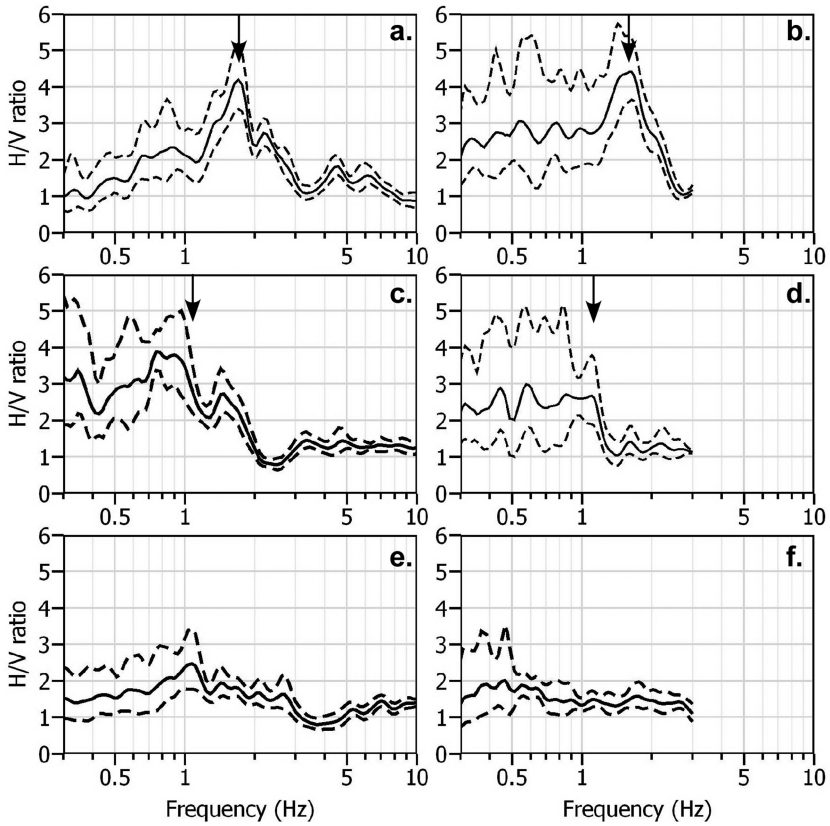

Figure 3. H/V curves. (a) Point P-03—measured real ambient noise. (b). Point P-03—simulated synthetic noise. (c) Point P-13—measured real ambient noise. (d) Point P-13—simulated synthetic noise. (e) Point T2–02—measured real ambient noise. (f) Point T2–02—simulated synthetic noise. Arrow: peak frequency.

exhibit two specific shapes according to the location within the valley. Downstream and upstream the Séchilienne basin, H/V curves present a well-defined single peak having amplitude greater than four over the 1.35–2 Hz and the 1.7–2.35 Hz frequency band, respectively (Figs 2a and 3a). Into the Séchilienne basin, H/V ratios exhibit a plateau-like shape with amplitude higher than three over a broad frequency band from 0.4 to 0.9–1.55 Hz (Figs 2a and 3c). Along the transverse profiles T1, T2 and T3, H/V curves exhibit also different shapes according to the station location. Downstream (profile T1, Fig. 2b) and upstream (profile T3, Fig. 2d) the Séchilienne basin, H/V ratios show a well-defined single peak with an amplitude greater than four, whatever the distance from the valley edge. On the contrary, into the Séchilienne basin (profile T2, Fig. 2c), even if a well-defined peak is observed in station T2–6, plateau-like shapes are found in the centre of the valley (T2–4 to T2–5) while 'almost flat' H/V curves with low H/V amplitudes (<2) are observed close to the basin edges (T2–1 to T2–3; Fig. 3e). Stations T2–7 to T2–10 show a more complicated shape in between a broad peak and plateau like-shape probably due to the presence of seismic sources (the road and the Romanche river), as well as a complex geological structure related to the alluvial fan (Figs 1 and 2c). The interpretation of recordings at these sensors is then difficult.

The observed different H/V curve shapes suggest variable complexity in wave propagation. Downstream and upstream the Séchilienne basin, the H/V curves fit the criteria proposed in the SESAME guideline for a 1-D resonance phenomenon (SESAME Deliverable D23.12 2005). In the Séchilienne basin, the plateau-like shapes in the valley centre and the flat H/V ratios near the valley edges could be caused by more complex wave propagation modes (2-D/3-D resonance, steep underground slopes), as already observed in real and simulated noise data (e.g. Uebayashi 2003; Guillier *et al.* 2006; Roten *et al.* 2006; Uebayashi *et al.* 2008; Bonnefoy-Claudet *et al.* 2009; Özalaybey *et al.* 2011).

Various sources of noise contribute to the noise wavefield in different frequency bands (Bonnefoy-Claudet *et al.* 2006b). While low-frequency seismic noise (<0.5 Hz) is most often produced by coastal wave and large-scale meteorological perturbations, seismic noise at frequencies above 1 Hz is related to human activities and, around 1 Hz, to local meteorological conditions (Bonnefoy-Claudet *et al.* 2006b). The energy content of the noise wavefield in the Romanche valley (between 0.5 and 10 Hz) suggests excitation by local meteorological conditions and human activities.

4 3-D MODEL NUMERICAL MODELLING OF AMBIENT NOISE

4.1 3-D model of the Romanche valley

Thanks to previous geophysical investigations carried out in the lower Romanche valley, including seismic reflexion prospecting (profile S1, Fig. 1b, Le Roux *et al.* 2010) and electrical resistivity tomographies (profiles E5 and E6, Fig. 1b, Le Roux 2011), the bedrock depth (H) is constrained into and upstream the Séchilienne basin. Bedrock depth was found to vary from 330 to 370 m in the Séchilienne basin centre (profile S1, lozenges; Fig. 4a), while, in the upstream part of the valley, it deepens from 10 to 20 m near the southern edge (profile E6, squares; Fig. 4d) to at least 120 m in the centre (profile E5, arrow, Fig. 4a). A power-law relationship was thus derived between bedrock depth (H) and H/V peak frequency

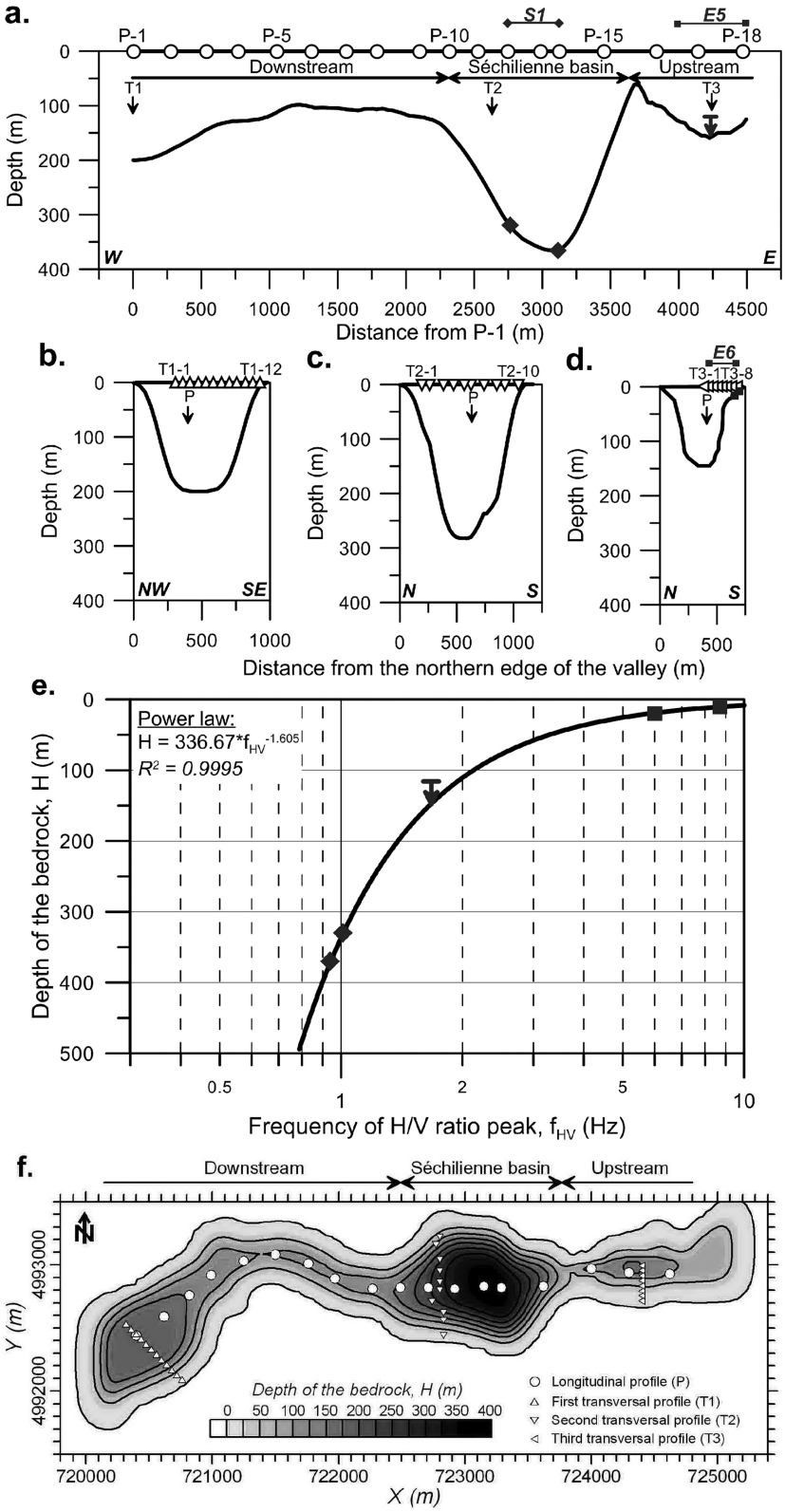

Figure 4. Bedrock depth along (a) profile P, (b) profile T1, (c) profile T2 and (d) profile T3. (e) Comparison between bedrock depth (H) inferred from seismic reflexion investigations (profile S1, lozenges, Le Roux *et al.* 2010) and electrical resistivity tomographies (profile E5, arrow and profile E6, squares, Le Roux 2011) and the H/V peak frequencies (f_{HV}). (f) 3-D bedrock depth model of the lower Romanche valley used in the numerical simulation with the location of the ambient noise measurements.

(f_{HV}) (Fig. 4e) along the longitudinal profile P (Fig. 2a). Similar power-law relationships between f_{HV} and H (whose parameters depend on the type of sediments and relies on a spatial homogeneity of sediments) have already been proposed by other authors (Ibs-von Seht & Wohlenberg 1999; Delgado *et al.* 2000; Parolai *et al.* 2002; Benjumea *et al.* 2011; Özalaybey *et al.* 2011). Such a correlation is supported by the observation that the shear wave velocity in unconsolidated overburden commonly exhibits a gradient with depth. This experimental law was then used to estimate the bedrock depth at the 18 sites of the longitudinal profile (P-1 to P-18, Fig. 1b). The resulted cross-section is displayed in Fig. 4(a). Assuming a smoothed U-shape valley with a trapezoidal angle of 30°, which is often observed in glacial alpine valleys (MacGregor *et al.* 2000; Lacave & Lemeille 2006) and is suggested in the transverse T1 and T3 profiles (Figs 2b and d), H was then computed along several transverse profiles. This assumption could generate a higher uncertainty of the model near the edge of the valley. In particular, the cross-sections of profiles T1–T3 are given in Figs 4(b) to (d). Finally, a 3-D geometry of the lower Romanche valley (Fig. 4f) was built by applying the Natural Neighbour gridding method (Watson & Philip 1987).

4.2 3-D numerical modelling of ambient vibration

The 3-D numerical model was defined by the geometry and the mechanical properties (*P*- and *S*-wave velocities, *P*- and *S*-quality factors and density) of sedimentary layers and underlying bedrock. In the Romanche valley, seismic investigation including *P*- and *S*-wave seismic refraction, surface wave analysis and seismic reflexion has shown that sediments can be described by six horizontally homogeneous layers overlaying a rigid bedrock (Le Roux 2009; Le Roux *et al.* 2010; Table 1). The depth of these layers is kept constant in the whole 3-D model. This assumption could generate some velocity errors near the edges of the valley, where lateral facies variations are expected (alluvial fans, scree deposits). Ambient noise simulation was performed with the NOISE code developed within the *SESAME* project (Kristek *et al.* 2002; Moczo & Kristek 2002; Moczo *et al.* 2002; Kristek & Moczo 2003), which is not able to treat non-planar free surface boundary conditions and thus surface topography. Ground motion modelling performed in the Grenoble valley, which is very close to the Séchilienne basin, has shown that effects of free-surface topography were found very small within the valley (Chaljub *et al.* 2010). We thus assume in this paper the lack of topography as being an acceptable approximation for ambient noise modelling. Noise sources are modelled by a set of randomly distributed single body forces located at the surface and having random direction, time function and maximum amplitude. Generated waves are then propagated by using an explicit heterogeneous finite-difference scheme, which is fourth-order accurate in space and second-order accurate in time. The FD-grid is staggered and consists of a finer grid on top and a coarser grid below. We used $447 \times 447 \times 16$ grid cells in the north, east and vertical directions for the fine grid, and $149 \times 149 \times 154$ grid cells for the coarse grid, with a grid cell size of 30 and 90 m, respectively. The grid size along the x-axis is twice as large as the basin length, ensuring numerical stability and non-reflecting boundaries are applied at the grid limits (Moczo *et al.* 2002). Fig. 4(f) shows a zoom on the 3-D valley model with the location of receivers. The simulations were performed in the frequency range from 0.33 to 2.94 Hz with a time step of 0.0035 s and resulted in 7 min of noise synthetics. The explicit staggered-grid finite-difference scheme used in this paper (Moczo *et al.* 2002, 2007) includes harmonic averaging of the bulk and shear moduli and volume arithmetic averaging of density, which allows computing effective grid material parameters. In this study, the effective minimum shear wave velocity is about 710 m s^{-1}, which allows accurately propagating Rayleigh and Love surface waves up to about 3 Hz. Forty eight receivers were distributed at the valley surface (Fig. 4e), at the same location as single-station ambient noise measurements (Fig. 1b). The computation of 7 min of noise synthetics required about 160 hr of CPU time. H/V spectral ratio computations from noise synthetics were also performed using the Geopsy software (see details in Section 3). Records are cut in time windows of 60 s duration length. The H/V ratio at each station is then obtained by averaging the H/V ratios of seven windows.

5 DISCUSSION AND INTERPRETATION

5.1 Validation of the 3-D model

H/V profiles derived from noise synthetics are displayed in Fig. 5, similarly to the empirical results presentation (Fig. 2). Even if amplitudes of the H/V peaks are lower (maximum of 4) than those obtained on real noise (maximum of 6), one may observe an excellent correlation between synthetic and real H/V curves in the centre of the valley. However, some differences are underlined near the edges of the valley on the transverse profiles T1 and T3. Along these profiles, the measured H/V frequencies are close or higher than 3 Hz, which is the upper frequency limit in the numerical simulations. That could explain a part of the discrepancy. However, an increase of the measured peak frequencies (and <3Hz) is observed at some sensors near the edges, which is not visible on the computed H/V ratios. This difference can result from the high uncertainties on the model geometry and on the seismic velocity values at the valley edges. Consistency of H/V peak frequencies determined from real and synthetic noise (f^M_{HV} and f^S_{HV}, respectively) is underlined in

Table 1. Geophysical and geological model of the Romanche valley inferred from seismic investigations (Le Roux 2009; Le Roux *et al.* 2010). α, *P*-wave velocity; β, *S*-wave velocity; Q_α, quality factor of *P* wave; Q_β, quality factor of *S* wave; ρ, mass density; H, depth of the bedrock.

Depth (m)	α (m s^{-1})	β (m s^{-1})	Q_α	Q_β	ρ (kg m^{-3})	Geological interpretation
0 to 10 or H	600	300	50	25	1900	Glaciolacustrine deposits
10 to 20 or H	1400	600	50	25	1900	Saturated glaciolacustrine deposits
20 to 120 or H	2200	800	50	25	1900	Saturated glaciolacustrine or subglacial deposits
120 to 170 or H	2300	840	50	25	1900	Saturated glaciolacustrine or subglacial deposits
170 to 270 or H	2400	880	50	25	1900	Saturated glaciolacustrine or subglacial deposits
270 to H	2500	920	50	25	1900	Saturated glaciolacustrine or subglacial deposits
>H	4000	2000	400	200	2500	Bedrock

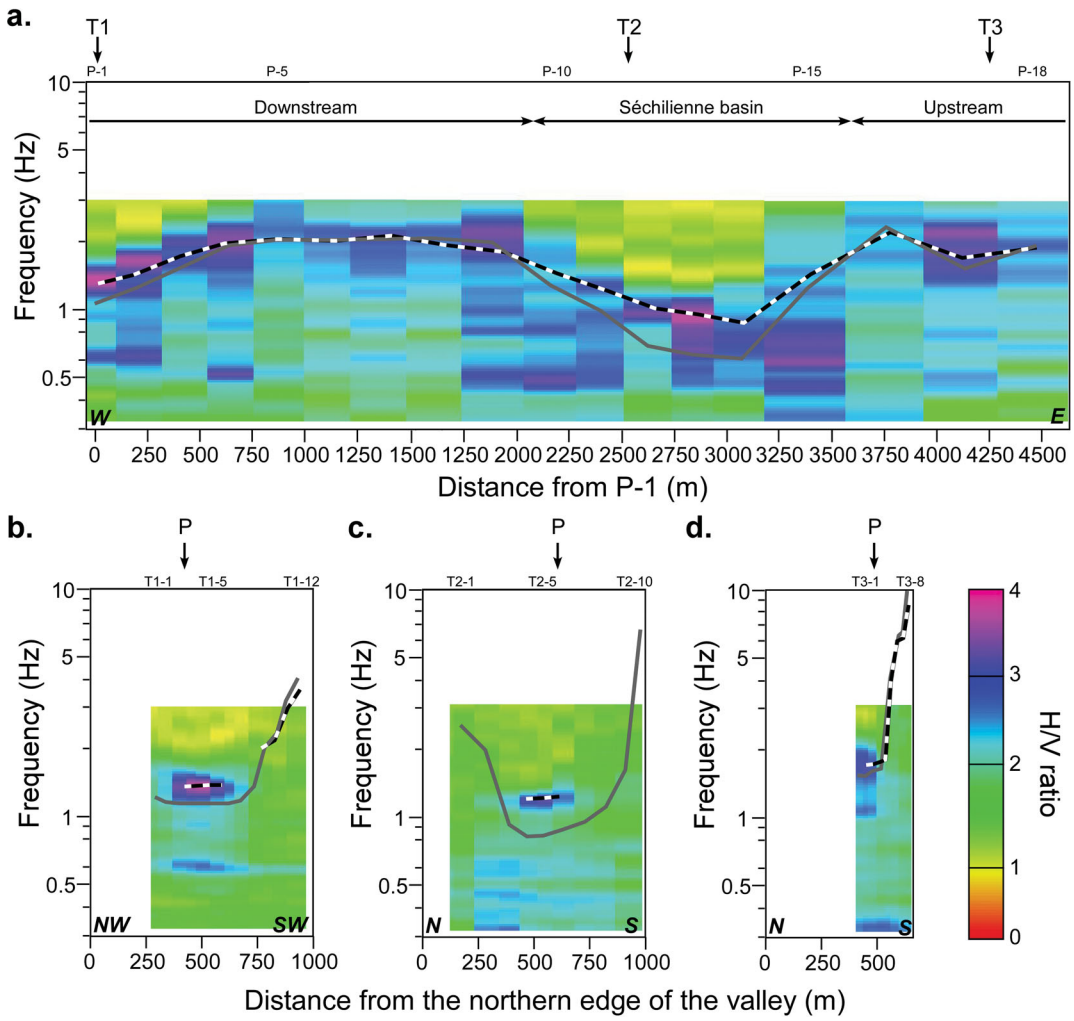

Figure 5. H/V spectral ratios computed from noise synthetics. (a) Longitudinal H/V profile along the Romanche valley (profile P). (b) First transversal H/V profile (profile T1). (c) Second transversal H/V profile (profile T2). (d) Third transversal H/V profile (profile T3). Dotted line: H/V peak frequency derived from the analysis of real microtremors (f_{HV}^{M}). Grey continue line: 1-D resonance frequency ($f_0^{1\text{-D}}$, Dobry *et al.* 1976).

Fig. 6. Only the sensors where empirical H/V peaks were visible are indicated in Fig. 6. For H/V curves exhibiting a plateau-like shape, the H/V peak frequency was defined as the cut-off frequency of the plateau (Guillier *et al.* 2006). For the longitudinal profile, the relative difference between the two frequencies is lower than 5 per cent. Moreover, H/V curves derived from real and synthetic noise (Fig. 3) exhibit quite similar shapes: well-defined H/V peaks downstream and upstream the Séchilienne basin (Figs 3a and b), plateau-like shapes in the centre of the Séchilienne basin (Figs 3c and d) and almost flat H/V curves close to the edge of the Séchilienne basin (Figs 3e and f). These results strongly validate the 3-D numerical model of the lower Romanche valley, which was simply obtained by correlating bedrock depth inferred at few sites by geophysical methods with the corresponding H/V peak frequencies, using a power law. Interestingly, in this paper, the power-law relationship was determined without any consideration about the wave propagation complexity (1-D, 2-D, 3-D) in play, which opens perspective of application in complex basin structure, provided however a spatial homogeneity of sediment infilling. However, the relationship must be determined in the valley centre (where the sediment thickness is maximum) to exclude the possibility of biased relationships in case of 2-D resonances.

5.2 Wave propagation in the Romanche valley

To better understand the wave propagation in the Romanche valley, we have compared the measured H/V peak frequencies (f_{HV}) with resonance frequencies computed for 1-D structure and 2-D structure. By using the formulation proposed by Dobry *et al.* (1976), the theoretical resonance frequency ($f_0^{1\text{-D}}$) was computed at each measurement site (Fig. 5). While an excellent agreement is found between $f_0^{1\text{-D}}$ and f_{HV} downstream and upstream the Séchilienne basin, f_{HV} drastically overestimates $f_0^{1\text{-D}}$ by about 40 per cent into the Séchilienne basin and by about 20 per cent in the deepest part of the downstream area. This clearly suggests mainly 1-D wave propagation downstream and upstream the Séchilienne basin and a more complex pattern into the Séchilienne basin and the deepest part of the downstream area. Bard & Bouchon (1985) defined a critical shape ratio for discriminating valleys affected by 2-D resonances from those characterized by 1-D resonance and lateral propagation of surface waves. Their criterion is based on the valley shape ratio, defined as the ratio between the total thickness of the sediments and the width over which the sediment thickness is greater than half its maximum value, and the *S*-wave velocity contrast between bedrock and sediments. For a given velocity contrast wave propagation will

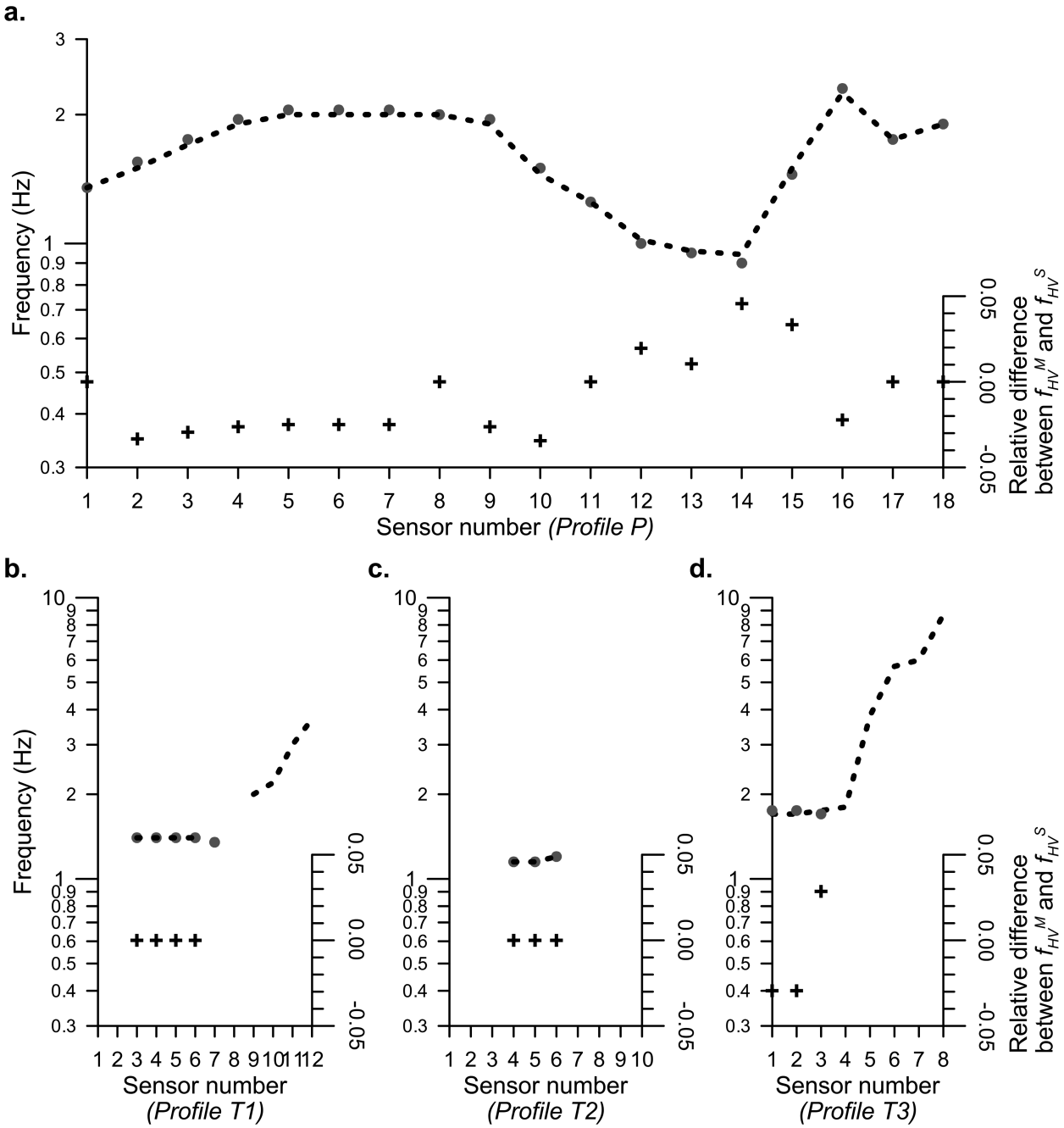

Figure 6. Comparison between H/V peak frequencies from real noise (f_{HV}^{M}, dark dotted line) and noise synthetics (f_{HV}^{S}, grey circles) and relative difference between f_{HV}^{M} and f_{HV}^{S} (crosses) for (a) profile P, (b) profile T1, (c) profile T2 and (d) profile T3.

be dominated by 2-D resonances for valleys with shape ratios larger than the critical value (dark line, Fig. 7). Given the 3-D model (Fig. 4f), we computed the shape ratio of the valley considering four areas: the shallowest and deepest part of the downstream area, into and upstream the Séchilienne basin (Fig. 7). From this simple criteria, the seismic wave propagation should be dominated by 1-D resonance and laterally propagating surface waves in the upstream and the shallowest part of the downstream area into the Séchilienne basin, while 2-D resonance should slightly affect the deepest part of the downstream area and strongly dominate in the Séchilienne basin. If 3-D resonance would occur in the Séchilienne basin, the H/V frequencies should be similar between sensors P-10 to P-14 and linked to the maximum depth of the basin (Rial 1989), which is not observed here (Fig. 2a).

Using the technique from Aki & Larner (1970), Bard & Bouchon (1985) simulated the seismic behaviour of a 2-D sine-shaped valley on incident *SH*, *SV* and *P* waves. The valley geometry is defined by its maximum thickness H_{M} and its mid-depth width W (Fig. 8). The terms transverse and axial are used for horizontal motion perpendicular and parallel to the valley axis, respectively (Field 1996). Bard & Bouchon (1985) showed the existence of three fundamental resonance modes (*SH*, *SV* and *P* modes) and proposed to estimate the 2-D resonance frequencies ($f_{SH}^{2\text{-D}}$ and $f_{SV}^{2\text{-D}}$ for the *SH* and *SV* fundamental modes corresponding to motion parallel and

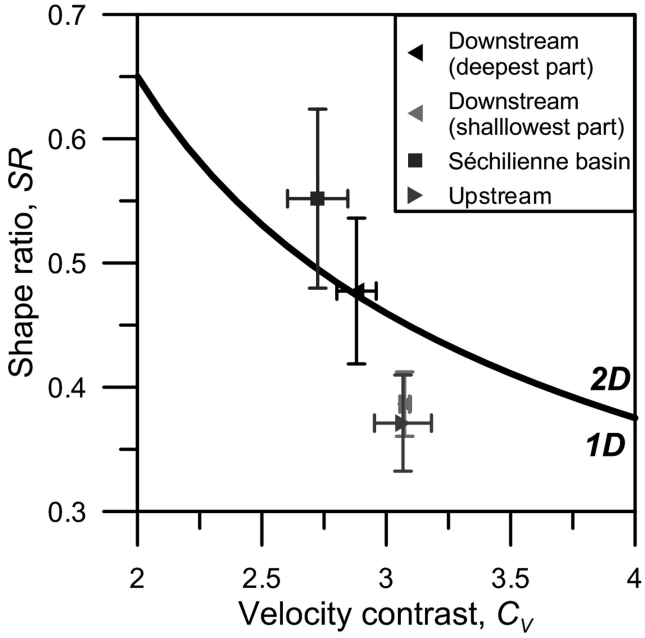

Figure 7. Critical shape ratio (dark line) as a function of the velocity contrast for the SH case (Bard & Bouchon 1985). The central point corresponds to the average for all sensors located in the given area (deepest and shallowest part of the downstream area, Séchilienne basin, upstream) and the error-bars are ± the standard deviation.

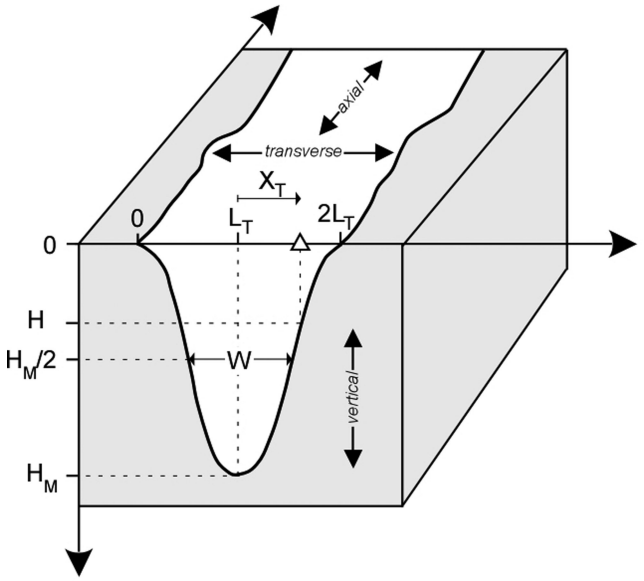

Figure 8. Schematic cross-section of a sine shaped valley with the convention used in the text (modified from Field 1996). Triangle, microtremor measurement; $2L_T$, transversal width of the valley; H_M, maximal depth of the bedrock; H, depth of the bedrock below the microtremor measurement; W, width of the valley at $H_M/2$; X_T, transversal distance between the centre of the valley and the microtremor measurement.

perpendicular to the valley axis, respectively), using the following equations:

$$f_{SH}^{2\text{-D}} = f_0^{1\text{-D}} c \sqrt{1 + \frac{H_M^2}{\left(\frac{W}{2}\right)^2}} \quad (1)$$

$$f_{SV}^{2\text{-D}} = f_0^{1\text{-D}} c \sqrt{1 + \left(\frac{2.9 H_M}{W}\right)^2}, \quad (2)$$

where $f_0^{1\text{-D}}{}_C$ is the 1-D resonance frequency at the valley centre.

These 2-D resonance frequencies are constant whatever the location along a profile across the valley (Bard & Bouchon 1985).

To check 2-D resonance in the Séchilienne basin, we computed spectral ratios of the Fourier amplitude spectra of the axial (parallel to the valley axis) over the vertical (A/V) components and the transverse (perpendicular to the valley axis) over the vertical component (T/V) separately, as suggested in Roten *et al.* (2006). The A/V and T/V peak frequencies determined on the synthetic noise (f_{AV}^S and f_{TV}^S, respectively) are displayed for profiles P (from P1–10 to P1–15) and T2 in Fig. 9, along with the theoretical 2-D fundamental *SH* and *SV* resonance modes ($f_{SH}^{2\text{-D}}$ and $f_{SV}^{2\text{-D}}$, respectively) estimated by Bard & Bouchon (1985).

The good agreement between the observed and 2-D theoretical resonance frequencies supports the 2-D resonance in the Séchilienne basin. On the contrary, theoretical 1-D resonance frequencies significantly underestimate observed frequencies (Fig. 9). Fig. 10 shows axial, transverse and vertical noise synthetics bandpass filtered around f_{AV}^S and f_{TV}^S. On the axial and transverse components, motions are in phase whatever the location along the profile, and exhibit a maximum at the valley centre and a minimum at the valley edge. On the vertical component, a phase change is observed at the valley centre, receivers from one side of the valley moving out-of-phase compared to receivers from the other side. Vertical motion is minimum in the valley centre and at the edges. These observations are consistent with the behaviour predicted by theory in case of 2-D resonances (Bard & Bouchon 1985) and strongly support the 2-D resonance of the Séchilienne basin.

6 CONCLUSION

H/V spectral ratios technique is often used for imaging the underground bedrock depth assuming 1-D wave propagation, which occurs when the valley thickness H is much lower than its width W. In case of pronounced 2-D or 3-D geometries (i.e. when H and W are of the same order of magnitude), observational and numerical studies have outlined rather peculiar H/V curve shape and the limits of using the 1-D wave propagation assumption to extract quantitative information on the underground structure. To better investigate capabilities of H/V measurements in complex structure, we carried out a detailed comparison between ambient noise measurements and simulated noise in the lower Romanche valley (French Alps). Indeed, analysis of the shape ratio of this small-size valley (0.5–1 km wide) indicates that two different wave propagation mode depending on the location within the valley are expected: (i) 1-D resonance upstream and downstream the Séchilienne basin and (ii) 2-D resonance into the Séchilienne basin.

Without any assumption on the wave propagation type, correlation at few different sites in the central part of the valley between H/V peak frequencies and bedrock depth inferred from geophysical methods allowed to drive a power-law relationship between bedrock depth and H/V peak frequency, which was further used to build the 3-D model of the bedrock depth. H/V curves computed on real and synthetic noise obtained by 3-D numerical modelling exhibit quite similar H/V peak frequencies (within 5 per cent) and curve shape. These results validate the 3-D geometrical and geophysical characterisation of the valley inferred from subsurface geophysical

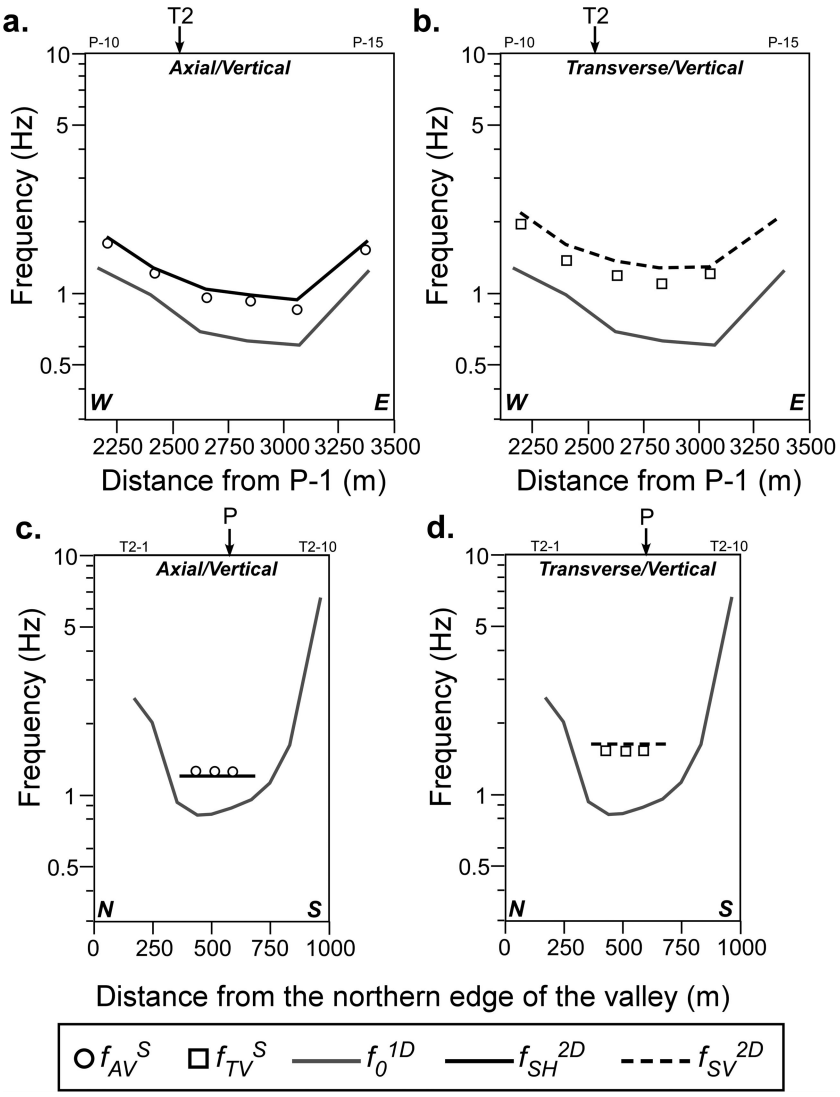

Figure 9. Simulated synthetic noise into the Séchilienne basin. (a) Longitudinal A/V profile along the Romanche valley (profile P). (b) Longitudinal T/V profile along the Romanche valley (profile P) (c) Second transversal A/V profile (profile T2). (d) Second transversal T/V profile (profile T2). Open white circle: peak frequency on the A/V spectral ratios computed from the simulated synthetic noise (f_{AV}^{S}). Open white square: peak frequency on the T/V spectral ratios computed from the simulated synthetic noise (f_{TV}^{S}) Grey continue line: 1-D resonance frequency ($f_0^{1\text{-D}}$, Dobry *et al.* 1976). Dark continue line: 2-D resonance frequency of SH mode ($f_{SH}^{2\text{-D}}$, Bard & Bouchon 1985). Dark dotted line: 2-D resonance frequency of SV mode ($f_{SV}^{2\text{-D}}$, Bard & Bouchon 1985).

prospecting and the ability of 3-D numerical scheme to capture main features of actual H/V observations.

The real and modelled H/V curves show a shape clearly different, depending on the location within the valley. In the shallowest part of the downstream area and upstream the Séchilienne basin, a well-defined peak is observed on the H/V spectral ratios with an amplitude greater than four, which can be observed from the centre to the edge of the valley. The H/V peak frequencies are in good agreement with the 1-D fundamental resonance frequency of the site, which confirms that wave propagation is mainly 1-D and the usefulness of using H/V peak frequencies for geometrical or geophysical quantitative characterisation of the valley. H/V curves in the Séchilienne basin do not exhibit a well-defined peak but an amplitude higher than three over a wide low-frequency band (plateau-like shape) in the centre of the valley and show almost flat curves at the edge of the valley, which confirms past numerical or observational evidences (Uebayashi 2003; Guillier *et al.* 2006; Roten *et al.* 2006; Bonnefoy-Claudet *et al.* 2009; Benjumea *et al.* 2011). In the centre, the H/V peak frequency overestimates by more than 40 per cent the 1-D theoretical resonance frequency. Computation of H/V by rotating the horizontal components along and perpendicular to the valley axis allow to clearly identify the fundamental mode of *SH* and *SV* 2-D resonances, which are in close agreement with theoretical values (Bard & Bouchon 1985).

At the end of this study we propose a strategy for the application of the H/V technique in case of deep basins. First, microtremor measurements along several profiles perpendicular to the valley axis should be performed. If similar H/V frequencies in the valley centre and flat H/V ratios near the valley edges are observed in such perpendicular profiles, 2-D resonance might occur. In this case, the application of the H/V technique, assuming 1-D wave propagation, might generate huge errors in the estimation of sediments depth. Instead, H/V ratios should be computed after rotating the horizontal components along and perpendicular to the valley axis to identify the fundamental mode of *SH* and *SV* 2-D resonance frequencies. It is then possible to calculate the real sediment depth

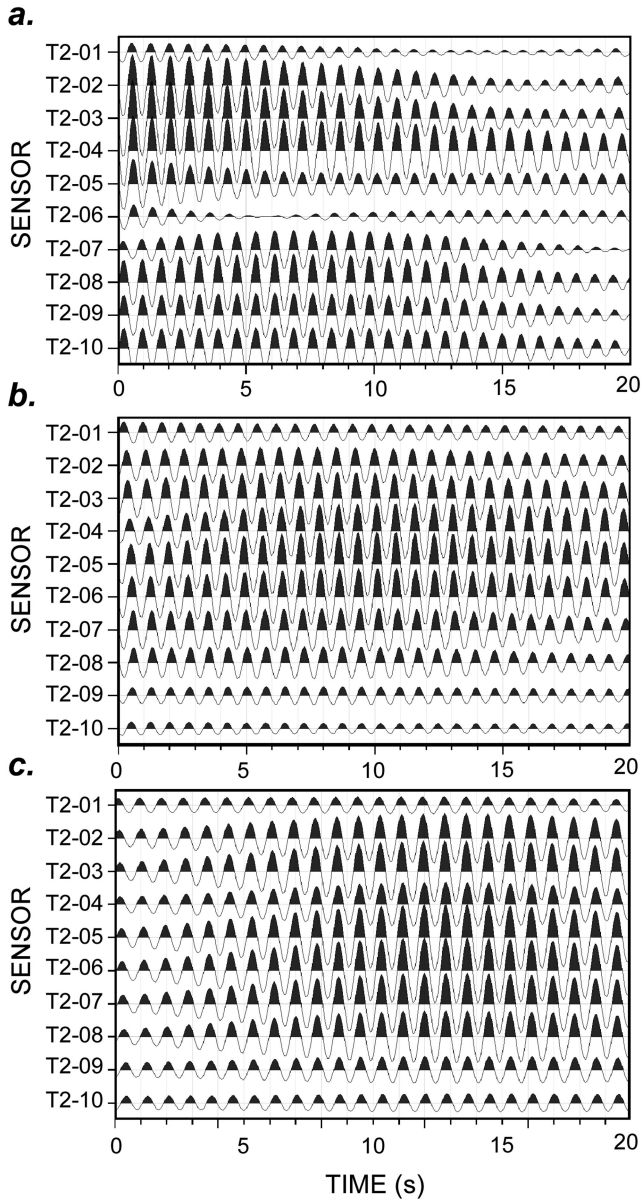

Figure 10. Bandpass filtered synthetic ambient noise records for all points on profile T2 along the (a) vertical component, (b) transverse component and (c) axial component (see Fig. 8). The bandpass filter was applied around the *SH* and *SV* fundamental mode frequencies: between 1.3 and 1.4 Hz for the vertical and perpendicular components, and between 1.15 and 1.25 Hz for the axial component.

using eqs (1) and (2) by estimating the width at mid-depth of the valley.

Beyond showing that observed and modelled H/V peak frequencies are similar and related to different wave propagation modes, this study also demonstrates the amount of information contained in the shape of the H/V curve. Indeed, analysis of H/V curve shape together with directional dependence of H/V peak frequencies may allow complexities of the underlying structure (e.g. steep underground slope, 2-D resonances, closeness to the valley edge) to be identified. We believe that this opens perspectives for making full use of the H/V curve for the inversion of complex ground structures.

ACKNOWLEDGMENTS

We gratefully acknowledge Matt Haney and an anonymous reviewer for their helpful comments.

REFERENCES

Albarello, D. & Lunedei, E., 2009. Alternative interpretations of horizontal to vertical spectral ratios of ambient vibrations: new insights from theoretical modelling, *Bull. Earthq. Eng.,* **8,** 519–534, doi:10.1007/s10518-009-9110-0.

Aki, K. & Larner, K.L, 1970. Surface motion of a layered medium having an irregular interface due to incident plane SH waves, *J. geophys. Res.,* **75,** 933–955.

Bard, P.Y., 1998. Microtremor measurements: a tool for site effect estimation?, in *Proceeding of the Second International Symposium on the Effects of Surface Geology on Seismic Motion,* Yokohama, Japan, Vol. 3, pp. 1251–1279.

Bard, P.Y. & Bouchon, M., 1985. The two-dimensional resonance of sediment-filled valleys, *Bull. seism. Soc. Am.,* **75,** 519–541.

Barféty, J.C., Bordet, P., Carme, F., Debelmas, J., Meloux, M., Montjuvent, G., Mouterde, R. & Sarrot-Reynauld, J., 1972. *Carte géologique de la France (1/50.000)*, feuille Vizille (797), BRGM, Orléans.

Benjumea, B., Macau, A., Gabàs, F., Bellmunt, F., Figueras, S. & Cirés, J., 2011. Integrated geophysical profiles and H/V microtremor measurements for subsoil characterization, *Near Surf. Geophys.,* **9,** 413–425, doi:10.3997/1873-0604.2011021.

Bièvre, G., Kniess, U., Jongmans, D., Pathier, E., Schwartz, S., van Westen, C., Villemin, T. & Zumbo, V., 2011. Paleotopographic control of landslides in lacustrine deposits (Trièves plateau, French western Alps), *Geomorphology,* **125,** 214–224.

Bindi, D. *et al*., 2009. Site amplifications observed in the Gubbio Basin, Central Italy: hints for lateral propagation effects, *Bull. seism. Soc. Am.,* **99,** 741–760, doi:10.1785/0120080238.

Bonnefoy-Claudet, S., Cornou, C., Bard, P.Y., Cotton, F., Moczo, P., Kristek, J. & Fäh, D., 2006a. H/V ratio: a tool for site effects evaluation. Results from 1D noise simulations, *Geophys. J. Int.,* **167,** 827–837.

Bonnefoy-Claudet, S., Bard, P.Y. & Cotton, F., 2006b. The nature of noise wavefield and its applications for site effects studies. A literature review, *Earth-Sci. Rev.,* **79,** 205–227.

Bonnefoy-Claudet, S., Baize, S., Bonilla, L.F., Berge-Thierry, C., Pasten, C., Campos, J., Volant, P. & Ferdugo, R., 2009. Site effect evaluation in the basin of Santiago de Chile using ambient noise measurements, *Geophys. J. Int.,* **176,** 925–937, doi:10.1111/j.1365-246X.2008.04020.x.

Chaljub, E., Moczo, P., Tsuno, S., Bard, P., Kristek, J., Kaser, M., Stupazzini, M. & Kristekova, M., 2010. Quantitative comparison of four numerical predictions of 3D ground motion in the Grenoble Valley, France, *Bull. seism. Soc. Am.,* **100**(4), 1427–1455.

Chávez-Garcia, F.J., Raptakis, D., Makra, K. & Pitilakis, K., 2000. Site effects at Euroseistest-II. Results from 2D numerical modelling and comparison with observations, *Soil Dyn. Earthq. Eng.,* **19**(1), 23–39.

Chávez-Garcia, F.J., Castillo, J. & Stephenson, W.R., 2003. 3D site effect; a thorough analysis of a high-quality dataset, *Bull. seism. Soc. Am.,* **92,** 1941–1951.

Cornou, C. & Bard, P.Y., 2003. Site-to-bedrock over 1D transfer function ratio: an indicator of the proportion of edge- generated surface waves?, *Geophys. Res. Lett.,* **30,** 1453–1457.

Delgado, J., Lopez Casado, C., Estevez, A.C., Giner, J., Cuenca, A. & Molina, S., 2000. Mapping soft soils in the Segura river valley (SE Spain): a case study of microtremors as an exploration tool, *J. appl. Geophys.,* **45,** 19–32.

Di Giulio, G., Cornou, C., Ohrnberger, M., Wathelet, M. & Rovelli, A., 2006. 2-D small aperture arrays for velocity profiles estimation using ambient seismic noise in a small-size alluvial basin (Colfiorito, Italy), *Bull. seism. Soc. Am.,* **96,** 1915–1933, doi:10.1785/0120060119.

Dobry, R., Oweis, I. & Urzua, A., 1976. Simplified procedures for estimating the fundamental period of a soil profile, *Bull. seism. Soc. Am.,* **66**(4), 1293–1321.

Field, E.H., 1996. Spectral amplification in a sediment-filled valley exhibiting clear basin-edge-induced waves, *Bull. seism. Soc. Am.,* **86,** 991–1005.

Guéguen, P., Cornou, C., Garambois, S. & Banton, J., 2007. On the limitation of the H/V spectral ratio using seismic noise as an exploration tool: application to the Grenoble Valley (France), a small apex ratio basin, *Pure appl. Geophys.,* **164,** 115–134.

Guillier, B., Cornou, C., Krister, J., Moczo, P., Bonnefoy-Claudet, S., Bard, P.Y. & Fäh, D., 2006. Simulation of seismic ambient vibrations: does the H/V provide quantitative information in 2D-3D structures?, in *Third International Symposium on the Effects of Surface Geology on Seismic Motion Grenoble,* France, 2006 September 1–August 28, 185pp.

Guillot, S., di Paola, S., Ménot, R.P., Ledru, P., Spalla, I., Gosso, G. & Schwartz, S., 2010. Suture zones and importance of strike-slip faulting for variscan geodynamic reconstructions of External Crystalline Massifs of western Alps, *Bulletin de la Société Géologique de France,* **6,** 483–500.

Graves, R.W., Pitarka, A. & Somerville, P.G., 1998. Ground motion amplification in the Santa Monica Area: effects of shallow basin edge structure, *Bull. seism. Soc. Am.,* **88,** 1224–1242.

Haghshenas, E., Bard, P.Y., Theodulidis, N., SESAME WP04 Team, 2008. Empirical evaluation of microtremor H/V spectral ratio, *Bulletin of Earthquake Engineering,* **6,** 75–108.

Hinzen, K.G., Scherbaum, F. & Weber, B., 2004. On the resolution of H/V measurements to determine sediment thickness, a case study across a normal fault in the Lower Rhine Embayment, Germany, *Journal of Earthquake Engineering,* **8,** 909–926.

Ibs-von Seht, M. & Wohlenberg, J., 1999. Microtremor measurements used to map thickness of soft sediments, *Bulletin of Seismological Society of America,* **89,** 250–259.

Kawase, H., 1996. The cause of the damage belt in Kobe: "The Basin- Edge Effect," constructive interference of the direct S-wave with the basin-induced diffracted/Rayleigh waves, *Seismological Research Letters,* **67,** 25–34.

Konno, K. & Ohmachi, T., 1998. Ground motion characteristics estimated from spectral ratio between horizontal and vertical components of microtremor, *Bull. seism. Soc. Am.,* **88**(1), 228–241.

Kristek, J., Moczo, P. & Archuleta, R., 2002. Efficient methods to simulate planar free surface in the 3D 4th-order staggered-grid finite difference schemes, *Studia Geophysica et Geodaetica,* **46,** 355–381.

Kristek, J. & Moczo, P., 2003. Seismic wave propagation in viscoelastic media with material discontinuities – a 3D 4th-order staggered-grid finite-difference modelling, *Bull. seism. Soc. Am.,* **83,** 2273–2280.

Lacave, C. & Lemeille, F., 2006. Seismic hazard and alpine valley response analysis: Generic valley configurations, in *Proceedings of the 1st European Conference on Earthquake Engineering and Seismology,* Geneva, Switzerland.

Le Roux, O., 2009. Caractérisation de l'évolution géomorphologique de la basse vallée de la Romanche en relation avec les instabilités gravitaires de ses versants rocheux, contraintes morphologiques, géophysiques et géochronologiques, *PhD thesis,* Joseph Fourier University, Grenoble, 321 pp.

Le Roux, O., Schwartz, S., Gamond, J.F., Jongmans, D., Tricart, P. & Sebrier, M., 2010. Interaction between tectonic and erosion processes on the morphogenesis of an alpine valley: geological and geophysical investigations in the lower Romanche valley (Belledonne massif, western Alps), *Int. J. Earth Sci.,* **99,** 427–441, doi:10.1007/s00531-008-0393-1.

Le Roux, O., 2011. Caractérisation de l'évolution géomorphologique de la basse vallée de la Romanche en relation avec les instabilités gravitaires de ses versants rocheux, *Bull. Eng. Geol. Environ.,* **70,** 483–495, doi:10.1007/s10064-010-0325-8.

Lermo, J. & Chávez-García, F.J., 1994. Are microtremors useful in site response evaluation?, *Bull. seism. Soc. Am.,* **84,** 1350–1364.

Lunedei, E. & Albarello, D., 2010. Theoretical HVSR curves from full wavefield modelling of ambient vibrations in a weakly dissipative layered Earth, *Geophys. J. Int.,* **181,** 1093–1108, doi:10.1111/j.1365-246X.2010.04560.x.

MacGregor, K.R., Anderson, R.S., Anderson, S.P. & Waddington, E.D., 2000. Numerical simulations of glacial-valley longitudinal profile evolution, *Geology,* **28**(11), 1031–1034.

Malischewsky, P.G. & Scherbaum, F., 2004. Love's Formula and H/V-Ratio (Ellipticity) of Rayleigh Waves, *Wave Motion,* **40,** 57–67.

Moczo, P. & Bard, P.Y., 1993. Wave diffraction, amplification and differential motion near strong lateral discontinuities, *Bull. seism. Soc. Am.,* **83,** 85–106.

Moczo, P. & Kristek, J., 2002. FD code to generate noise synthetics, Deliverable of the SESAME European Project, D09.02.

Moczo, P., Kristek, J., Vavrycuk, V., Archuleta, R.J. & Halada, L., 2002. 3D heterogeneous staggered-grid finite-difference modelling of seismic motion with volume harmonic and arithmetic averaging of elastic moduli and densities, *Bull. seism. Soc. Am.,* **92,** 3042–3066.

Moczo, P., Robertsson, J. & Eisner, L., 2007. The finite-difference time-domain method for modeling of seismic wave propagation, *Adv. Geophys.,* **48,** 421–516.

Montjuvent, G. & Winistorfer, J., 1980. Glaciations quaternaires dans les Alpes franco-suisses et leur piedmont, *Geologie Alpine,* **56,** 251–28.

Nakamura, Y., 1989. A method for dynamic characteristics estimation of subsurface using microtremor on the ground surface, Quarterly Report of the Railway Technical Research Institute, Vol. 30, pp. 25–33.

Nogoshi, M. & Igarashi, T., 1972. On the amplitude characteristics of microtremor (Part 2), *J. seism. Soc. Japan,* **24,** 26–40.

Özalaybey, S., Zor, E. & Tapirdamaz, M.C., 2011. Investigation of 3-D basin structures in the İzmit Bay area (Turkey) by single- station microtremor and gravimetric methods, *Geophys. J. Int.,* **186,** 883–894.

Parolai, S., Bormann, P. & Milkert, C., 2002. New relationships between Vs, thickness of sediments, and resonance frequency calculated by the H/V ratio of seismic noise for Cologne Area (Germany), *Bull. seism. Soc. Am.,* **92,** 2521–2527.

Rial, J.A., 1989. Seismic wave resonances in 3-D sedimentary basins, *Geophys. J. Int.,* **99,** 81–90.

Roten, D., Fäh, D., Cornou, C. & Giardini, D., 2006. Two-dimensional resonances in Alpine valleys identified from ambient vibration wafefields, *Geophys. J. Int.,* **165,** 889–905.

Rovelli, A., Scognamiglio, L., Marra, F. & Caserta, A., 2001. Edge diffracted 1-sec surface waves observed in a small-size intramountain basin (Colfiorito, central Italy), *Bull. seism. Soc. Am.,* **91,** 1851–1866.

Sánchez-Sesma, F.J. & Luzón, F., 1995. Seismic response of three-dimensional alluvial valleys for incident P, S, and Rayleigh waves, *Bull. seism. Soc. Am.,* **85,** 269–284.

Sánchez-Sesma, F.J. *et al*., 2011. A theory for microtremor H/V spectral ratio: application for a layered medium, *Geophys. J. Int.,* **186,** 221–225.

SESAME Deliverable D23.12, 2005. Guidelines for the implementation of the H/V spectral ratio technique on ambient vibrations measurements, processing and interpretation, Deliverable of the SESAME European Project, D23.12. Université Joseph Fourier, Grenoble, France.

Tuan, T.T., Scherbaum, F. & Malischewsky, P.G., 2011. On the relationship of peaks and troughs of the ellipticity (H/V) of Rayleigh waves and the transmission response of single layer over half-space models, *Geophys. J. Int.,* **184,** 793–800.

Uebayashi, H., 2003. Extrapolation of irregular subsurface structures using the horizontal to vertical spectra ratio of long period microtremors, *Bull. seism. Soc. Am.,* **93,** 570–582.

Uebayashi, H., Kawabe, H., Kamae, K., Miyakoshi, K. & Horike, M., 2008. Behavior of microtremor H/V spectrum and phase velocity on the basin peripheral and inversion for determing basin structure, in *Proceedings of 14th World Conference Earthquake Engineering,* Beijing, China, pp. 02–37.

Wathelet, M., Jongmans, D., Ohrnberger, M. & Bonnefoy-Claudet, S., 2008. Array performances for ambient vibrations on a shallow structure and consequences over V_s inversion, *J. Seismol.,* **12,** 1–19.

Watson, D.F. & Philip, G.M., 1987. Neighborhood based interpolation, *Geobyte,* **2,** 12–16.